I.J. Wireless and Microwave Technologies, **2022, 3, 1-17**
Published Online June 2022 in MECS (http://www.mecs-press.org/)
DOI: 10.5815/ijwmt.2022.03.01

Propagation Channel Modeling for Low-Altitude Platform Non-Terrestrial Networks from 275 GHz to 3 THz

Kok Yeow You
School of Electrical Engineering, Faculty of Engineering, Universiti Teknologi Malaysia, Skudai, Johor, Malaysia
Email:kyyou@fke.utm.my, kyyou77@gmail.com

Received: 03 March 2022; Revised: 14 April 2022; Accepted: 02 May 2022; Published: 08 June 2022

Abstract: One of the important studies in 6G aerial radio access networks is the propagation channel modeling. The high accurate propagation channel model will save cost and time, and is more effective in the design of the air radio access network system. However, existing channel models are limited to 1 THz, while 6G wireless technology is expected to operate up to 3 THz. In this paper, the propagation channel from 275 GHz to 3 THz is modeled by modifying the Friis equation, and each parameter in the model is described and analyzed analytically. The main factors that contribute to wireless signal attenuation at terahertz, such as atmospheric oxygen and water vapor, rainfall, and cloud factors, are also discussed in detail. Furthermore, the propagation channel calculation App for 6G low-altitude platform access networks application has been built using MATLAB GUI.

Index Terms: Aerial radio access networks, cloud attenuation, Friis equation, low-altitude platforms, path loss, propagation channel model, rain attenuation, TeraHertz, water vapour attenuation, International Telecommunication Union ITU.

1. Introduction

As known that the terahertz frequencies radio access networks from 90 GHz to 3 THz will be practiced for 6G communication applications by 2030 to meet the growing needs of users, such as 0.1 – 1 Tbps of data rate, 3 – 60 bps/Hz of spectral efficiency, 100 GHz of channel bandwidth, and 1000 km/h of mobility [1]. Long distance terrestrial radio access networks (TRANs) are not suitable for implementation at terahertz (THz) frequencies because it will deal with high transmission path loss mainly due to atmospheric absorption and other environmental factors. For instance, at sea level, the atmospheric absorption loss is approximately 5 dB/km at 275 GHz and increases dramatically to 300 dB/km at 1 THz, as well as reaching 4000 dB/km at 3 THz [2]. Recently, low-altitude non-terrestrial networks (LANTN) are becoming an alternative method to solve the high loss problem for transmitted signal up to THz, since the signal attenuation decreases with the height of the sea level. The infrastructures of non-terrestrial communication stations are normally handled by unmanned aerial vehicles (UAVs) [3, 4].

Apart from communication applications, the LANTN are very useful in low-altitude Internet of Things (IoT), such as remote sensing applications [5]. For instance, agricultural remote sensing systems can help farm managers to detect large-scale soil moisture, monitor crop growth, monitor diseases and insect pests, apply pesticides and fertilize, thus achieving the goal of saving labor costs and time for farmland management as well as precision operation. Nevertheless, there are few studies on the path loss model above sea level up to THz. In fact, the path loss model is very important in the construction of the future LANTN at a specific frequency ant location above sea level. Through the path loss model, the amount of power to be transmitted, the wireless distance between the transmitting antenna and the receiving antenna, and the signal level that the receiver can receive can all be predicted before the actual construction of the LANTN.

In this work, a path loss model use to predict the signal attenuation of the LANTN (sea level height from 0 m to 5000 m and operating frequency from 275 GHz to 3 THz) is re-analyzed. In general, the received signal level, P_r (in logarithmic unit) at receive antenna due to path loss can be predicted using Friis's equation as [6]:

$$P_r = P_t + 10\log_{10}(G_t) + 10\log_{10}(G_r) - PL \tag{1}$$

where PL is the path loss of free-space as expressed in equation (4). On the other hand, G_t and G_r (in unit linear magnitudes) are the gain of the receive and transmit antennas, respectively. Symbol P_t is the transmitted power in logarithmic unit emitted from the transmit antenna. However, the origin Friis equation (1) does not take into account the transmitted signal losses due to height of sea level, gases absorption, and other weather factors. In this study, the Friis equation was modified to include attenuation factors caused by atmospheric oxygen and water vapor, rainfall, and clouds or snow as expressed in Eq. (2). Those attenuations as a function of frequency are re-formula based on the available calculated values and data from International Telecommunication Union ITU-R Reports [2], [7], and [8], respectively. In additional, the mentioned ITU-R reports only provides data and calculations up to 1 THz, whereas in this study, the applicable range of attenuation calculations is extended to 3 THz. Besides, a standalone MATLAB-based Guide User Interface (GUI) is developed for automated simulation of attenuation and received power, P_r. The receiver signal quality is also quantitatively evaluated using parameters, such as signal-to-noise ratio (SNR) (for analog receivers) and bit-error-rate (BER) (for digital receivers).

2. Propagation Channel Model

In this study, the propagation channel calculation is based on the Friis equation with considered the signal loss due to three main environmental factors, namely atmospheric gases, clouds, and rain, respectively. Hence, the signal power, P_r in unit dBm at the receiver is rewritten as:

$$P_r = P_t + 10\log_{10}\left(\chi_t G_t\right) + 10\log_{10}\left(\chi_r G_r\right) - PL - \left(\gamma_A \times \frac{d}{1000}\right) - \left(\gamma_R \times \frac{rd}{1000}\right) - \left(\gamma_C \times \frac{d}{1000}\right) \tag{2}$$

where P_r and P_t (in unit dBm) are the received power at the receive antenna and the transmitted power at the transmit antenna. Symbol d (in unit meter) is the horizontal distance between the transmitter and the receiver. Other parameters in Eq. (2) are described in Sub-section 2.1 to 2.5.

2.1 Antennas gain factor

The G_t and G_r (in unit linear magnitudes) in (2) are the gain of the receive and transmit antennas, respectively. The χ_t and χ_r are the gain reduction factors (gain decrease effect) for transmitter and receiver, respectively as [9]:

$$\chi_t = \begin{cases} 1-\xi\left(\dfrac{2\lambda G_t}{\pi^2 d}\right)^2 \\ 1-4\xi\left(\dfrac{2\lambda G_t}{\pi^2 d}\right)^2 \end{cases} \quad \text{and} \quad \chi_r = \begin{cases} 1-\xi\left(\dfrac{2\lambda G_r}{\pi^2 d}\right)^2 & \text{for} \quad G_t \text{ or } G_r \geq 10 \\ 1-4\xi\left(\dfrac{2\lambda G_r}{\pi^2 d}\right)^2 & \text{for} \quad G_t \text{ or } G_r < 10 \end{cases} \tag{3}$$

The ξ (≈ 0.06) is an empirical coefficient [9]. The traveling signal is affected by the gain reduction when the signal is transmitted from the transmitter to the receiver at close distance range (in the Fresnel zone). The gain values is usually between 2.15 dB to 80 dB. For instance, a dipole antenna has a gain of 2.15 dB, while a reflector antenna, such as the Herschel space observatory with a diameter dish of 3.5 m and an operating frequency of 450 GHz to 5 THz, has a gain of up to 70 dB.

2.2 Free-space path loss

The PL (in unit dB) is the path loss of free space between transmit and receive antennas as [6]:

$$PL(\text{dB}) = -147.5582 + 20\log_{10}(d) + 20\log_{10}(f) \tag{4}$$

where d (in unit meter) is the distance between the transmitter and the receiver. On the other hand, f (in unit Hz) is the operating frequency.

2.3 Atmospheric oxygen and water vapour attenuations

Although, data for variation in atmospheric attenuation, γ_A (in unit dB/km) with height above sea level, h and high operating frequency, f are available in ITU-R RA,2189-1 [2], but there are no formulas to relate the three parameters. In this study, the relationship of the three parameters are formulated using regression method. The γ_A as a function of height above sea level, h (in unit meter) and operating frequency, f (in unit Hz) is empirically expressed as:

$$\gamma_A = 10^{(a_1\times h+a_2)} f^4 - 10^{(a_3\times h+a_4)} f^3 + 10^{(a_5\times h+a_6)} f^2 - 10^{(a_7\times h+a_8)} f + 10^{(a_9\times h+a_{10})} \tag{5}$$

The ten constant values (a_1, a_2, a_3, a_4, a_5, a_6, a_7, a_8, a_9, and a_{10}) in Eq. (5) are fitted with the data extracted from ITU-R RA.2189-1 [2]. The model (5) is only applicable to a specific sub-frequency range from 275 GHz to 3 THz (see Tables A1 to A3 in Appendix A), in order to avoid the spectral "window" caused by the natural resonance of water vapour and oxygen molecules. In addition, the (5) is only valid for the range h from 0 km to 5 km. In fact, the rigorous study of atmospheric gases attenuation was initially reported by [10] and the model used, so-called line-by-line model, are re-documented in ITU-R P.676-12 [11]. Furthermore, the model has been packaged in the MATLAB function '`gaspl`'. However, this model is only applicable to 1 THz and does not involve variable of height above sea level, h, hence the new simple model of (5) is formulated and used in this study. The main differences between line-by-line model [10, 11] and (5) is tabulated in Table 1.

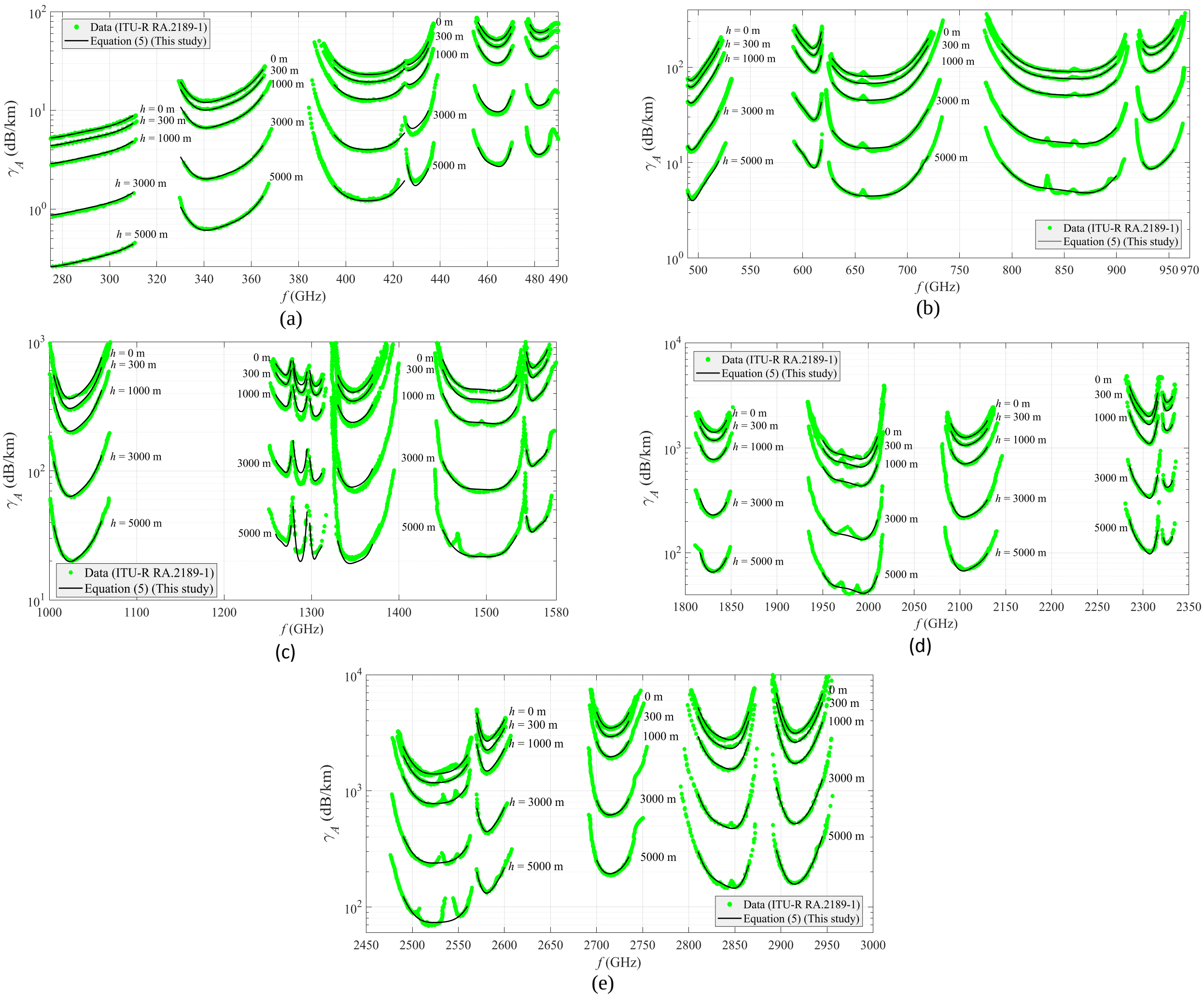

Fig. 1. Atmospheric attenuation, γ_A (dB/km) varies with altitude, h for frequency range of (a) 275 GHz to 490 GHz, (b) 500 GHz to 970 GHz, (c) 1000 GHz to 1580 GHz, (d) 1800 GHz to 2350 GHz, and (e) 2450 GHz to 3000 GHz

Table 1. Comparison of Features and Specifications Between Line-by-Line Model and Eq. (5)

Features and specifications	**Line-by-Line model [13, 14]**	**Eq. (5) (This study)**
Complexity	Rigorous	Simple
Operating frequency	1 GHz to 1 THz	275 GHz to 3 THz
Input parameters	a) Temperature, T b) Atmospheric pressure, P c) Water vapor density, ρ d) Transmit distance, d e) Frequency, f	a) Height above sea level, h b) Frequency, f
Attenuation analysis range	Entire frequency range includes the regions where oxygen and water vapor naturally resonate.	Separated sub-frequency range does not include the regions where oxygen and water vapor resonate.

2.4 Rain attenuation

The γ_R is the rain attenuation in unit dB/km due to rain rate at p percentage of time ($0.001\% \le p \le 1\%$) which is represented as power-law expression as [8]:

$$\gamma_R = \left\{0.12\, p^{-(0.546+0.043\log_{10} p)}\right\} k_H R_{0.01}^{\alpha} \tag{6}$$

where $R_{0.01}$ is the averaged rain rate (in unit mm/hour) at 0.01 percentage of time (p = 0.01%). In this study, the coefficients, k_H and α in (6) as function of operating frequency, f and capable of applying up to 3 THz compared to only 1 THz in recommendation ITU-R P.838-3 [8]. The coefficients, k_H and α are valid below 275 mm/h of $R_{0.01}$ as:

$$k_H = \kappa_1(\log_{10} f)^7 + \kappa_2(\log_{10} f)^6 + \kappa_3(\log_{10} f)^5 + \kappa_4(\log_{10} f)^4 + \kappa_5(\log_{10} f)^3 + \kappa_6(\log_{10} f)^2 + \kappa_7 \log_{10} f + \kappa_8 \tag{7a}$$

and

$$\alpha = A_1(\log_{10} f)^7 + A_2(\log_{10} f)^6 + A_3(\log_{10} f)^5 + A_4(\log_{10} f)^4 + A_5(\log_{10} f)^3 + A_6(\log_{10} f)^2 + A_7 \log_{10} f + A_8 \tag{7b}$$

The r is the path reduction factor proposed by International Telecommunication Union (ITU) which is given as [12]:

$$r = \frac{1}{1 + d/\left(35000 e^{-0.015 R_{0.01}}\right)} \tag{8}$$

It should be noted that coefficients k_H and α only for horizontal polarization. The fitting constant values of the k_H and α are listed in Table 2, which are obtained by fitting equations (7a) and (7b) with the calculated data in ITU-R P.838-3 [8]. Although the available data in ITU-R P.838-3 only limited to 1 THz, but the (7a) and (7b) are used to extrapolate the values up to 3 THz as shown in Fig. 2 (a) and (b), respectively. In addition, the γ_R data of ITU-R P.838-3 and literature data [13, 14] are consistent with the calculation using (6) assisted by (7a) and (7b) as shown in Fig. 2 (c).

From Fig. 2 (c), for $R_{0.01}$ = 150 mm/h, the attenuation, γ_R is varied from 35 dB/km to 50 dB/km for the frequency range from 275 GHz to 3 THz. When $R_{0.01}$ reaches an extreme value of 250 mm/h, the maximum value of γ_R is estimated to be 60 dB/km over the frequency range. In fact, the rain rate, $R_{0.01}$ value is not an observable fixed quantity, it depends on the region, season, and weather. For instance, the global average annual rainfall, $R_{0.01}$ distribution (p = 0.01%) has maximum $R_{0.01}$ of 90 mm/h in the tropical regions ($0^{o} \le {}^{o}\mathrm{N} < 22^{o}$). In middle latitudes ($22^{o} \le {}^{o}\mathrm{N} \le 45^{o}$) regions, the average value of $R_{0.01}$ is between 30 mm/h and 70 mm/h. Whereas, the $R_{0.01}$ value is less than 30 mm/h in polar latitudes ($> 45^{o}$ N) [15].

For a specific observation day or month, the $R_{0.01}$ value may exceed 200 mm/h. For instance, the tropical climate country, such as Malaysia, may have an average rainfall rate, $R_{0.01}$ of more than 150 mm/h during November [16]. In general, according to rain rate R value per hour or in a day, the type of precipitation can be determined, and vice versa [17, 18].

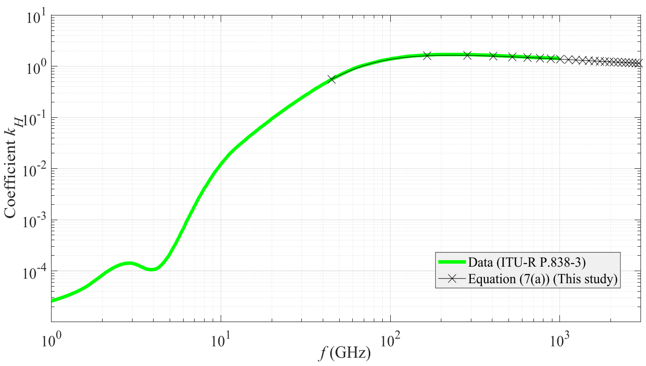

(a)

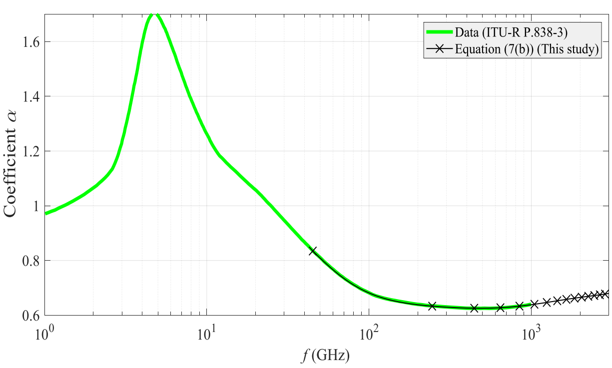

(b)

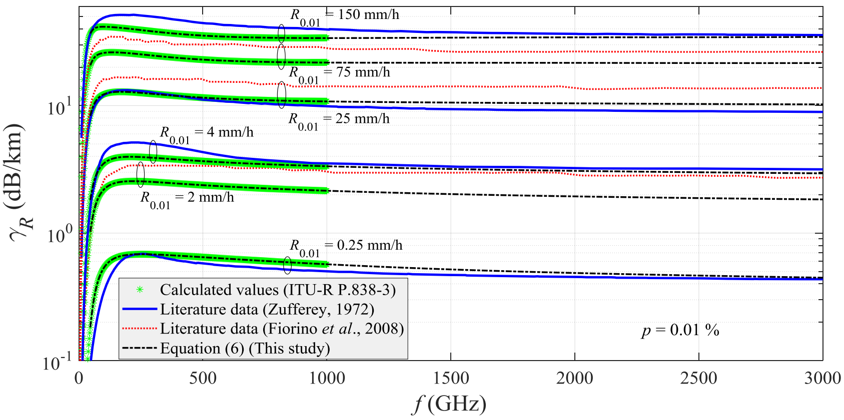

(c)

Fig. 2. (a) Coefficient, k_H and (b) coefficient, α over operating frequency from 1 GHz to 3 THz. (c) Comparison of rain attenuation, γR (dB/km) at various $R_{0.01}$ levels between literature values [8], [13, 14] and this study

Table 2. Coefficient values of Eqs. (7a) and (7b)

Coefficient, k_H [(dB/km)(mm/hour)$^{-\alpha}$]		Coefficient, α	
κ_1	-0.5922681720205624	A_1	0.1867273899361097
κ_2	48.77560212539895	A_2	-15.18476603103148
κ_3	-1720.713680092341	A_3	528.8744253816963
κ_4	33708.09238485347	A_4	-10226.86775418521
κ_5	-396000.7230266441	A_5	118576.5471629152
κ_6	2789884.071914158	A_6	-824361.0579617802
κ_7	-10913706.91296864	A_7	3181785.805109898
κ_8	18286922.01080923	A_8	-5259573.011800068

2.5 Cloud attenuation

The cloud attenuation, γ_C in unit dB/km in terms of liquid water content in the cloud, w (in unit g/m^3) proposed by ITU-R P.840-6 is given as [7], [19]:

$$\gamma_C = \frac{0.819\times10^{-9} f}{\varepsilon''_{r\_eff}\left[\left(\dfrac{\varepsilon'_{r\_eff}+2}{\varepsilon''_{r\_eff}}\right)^2+1\right]}\times w \tag{9}$$

where ε'_{r_eff} and ε''_{r_eff} are the effective dielectric constant and the loss factor of the mixture ice-water which can be calculated using two-component mixture model as [20]:

$$\varepsilon_{r\_eff} = \left[(1-v)\varepsilon^a_{r\_ice} + v\varepsilon^a_{r\_water}\right]^{\frac{1}{a}} = \varepsilon'_{r\_eff} - j\varepsilon''_{r\_eff} \tag{10}$$

For mixtures of different phase components, the empirical value of a in (10) is assumed to be 1/3, which conforms to the mixture model of Landau, Lifshitz and Looyenga [20]. The v is the volume fraction of the water liquid in cloud as [21, 22]:

$$v = \begin{cases} 1 & ,T \geq 0^{o}\text{C} \\ 1+\dfrac{T}{20} & ,-20 \leq T \leq 0^{o}\text{C} \\ 0 & T < -20^{o}\text{C} \end{cases} \tag{11}$$

The cloud droplets exist in water liquid form above 0 ℃ and a mixture of supercooled water and ice crystals between 0 ℃ to -20 ℃ depending on the type of cloud. Below than -20 ℃, the cloud droplets normally exist in ice crystal form. The relative complex permittivity, ε_{r_water} (= ε'_{r_water} - $j\varepsilon''_{r\_water}$) of water can be calculated from double-relaxation Debye model as [19]:

$$\varepsilon_{r\_water} = \varepsilon_2 + \frac{\varepsilon_0 - \varepsilon_1}{1 + j\left(\frac{f \times 10^{-9}}{f_p}\right)} + \frac{\varepsilon_1 - \varepsilon_2}{1 + j\left(\frac{f \times 10^{-9}}{f_s}\right)} \tag{12}$$

The parameters in Eq. (12) (for $f \leq 1$ THz) can be found in [19] and [7]. Although the ε_{r_water} of water has been studied for more than 80 years, there is a lack of permittivity data of water at THz and temperatures, T below 0 °C. In addition, there are deviations between the available ε_{r_water} data as shown in Fig. 3. By comparing (12) with literature data [23-25], the maximum deviation of $\Delta\varepsilon'_{r\_water}$ can reach 0.25, 0.42, and 0.45 at temperature of 20 °C, -2.05 °C, and -5.6 °C, respectively (covering the frequency range from 275 GHz to 3 THz). On the other hand, the maximum deviation of $\Delta\varepsilon''_{r\_water}$ is 1.0, 0.35, and 0.95 for 20 °C, -2.05 °C, and -5.6 °C, respectively. On the other hand, the dielectric constant, ε'_{r_ice} of ice is independent on operating frequency, f from few GHz to THz [26]. The temperature-dependent ε'_{r_ice} (for $T \leq 0$ °C) is given as [27]:

$$\varepsilon'_{r\_ice} = 3.1884 + 9.1 \times 10^{-4} T \tag{13}$$

While, the loss factor, ε''_{r_ice} of ice is increased with frequency up to 3 THz and empirically expressed as:

$$\varepsilon''_{r\_ice} = \left\{ \begin{aligned} &\left[\xi_9 \log_{10}(-T)^2 + \xi_8 \log_{10}(-T) + \xi_7\right] f^3 + \left[\xi_6 \log_{10}(-T)^2 + \xi_5 \log_{10}(-T) + \xi_4\right] f^2 \\ &+ \left[\xi_3 \log_{10}(-T)^2 + \xi_2 \log_{10}(-T) + \xi_1\right] f \end{aligned} \right\} \tag{14}$$

Eq. (14) are valid ranging 60 GHz to 3 THz and -0.1 °C to -170 °C. The fitting coefficients, ξ_n in (14) are tabulated in Table 3. Comparison of the accuracy of the calculated ε''_{r_ice} using (14) with the literature results [19], [26] is shown in Fig. 4.

By inserting (11), (12), (13), and (14) into (10), the values of ε'_{r_eff} and ε''_{r_eff} at different temperatures are calculated and plotted in Fig. 5. As expected, the values of ε'_{r_eff} and ε''_{r_eff} decrease with temperature, T and show three transitions in the ranges of $0^o \leq T < 40^o$, $-20^o \leq T < 0^o$, and $-40^o < T < -20^o$, respectively. At 1 THz, the value of ε'_{r_eff} decreases from 4.15 to 3.18 over range of -40 °C to 40 °C, that is, the maximum change of ε'_{r_eff} within the temperature range from 1 to 3 THz is almost 1 as shown in Fig. 5 (a). Whereas, the maximum deviation of the ε''_{r_eff} can reach 2.7 as shown in Fig. 5 (b).

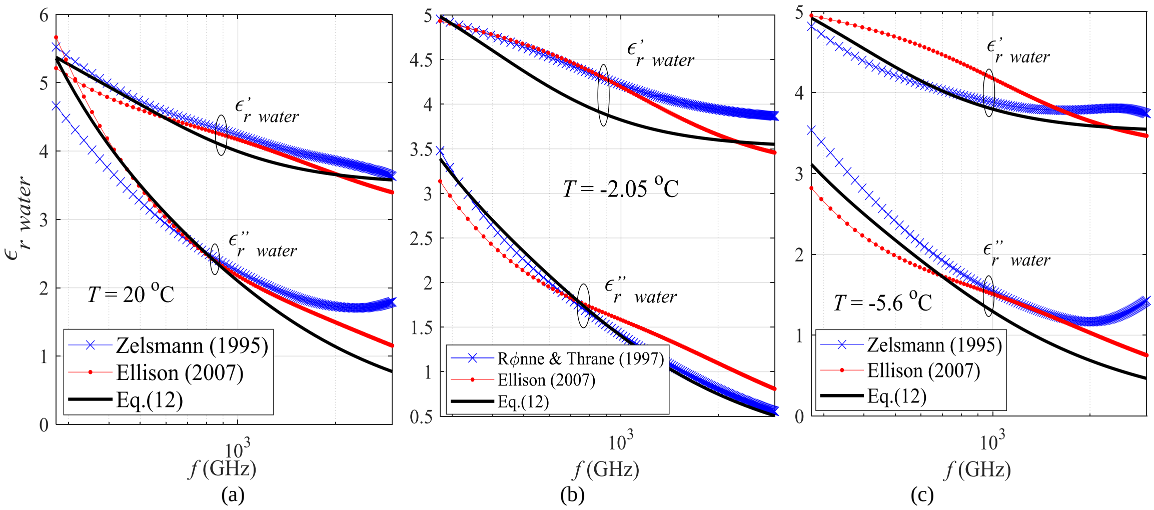

Fig. 3. Comparison calculated relative complex permittivity, ε_{r_water} of water and literature data from 275 GHz to 3 THz at (a) 20 °C, (b) -2.05 °C, and (c) -5.6 °C, respectively

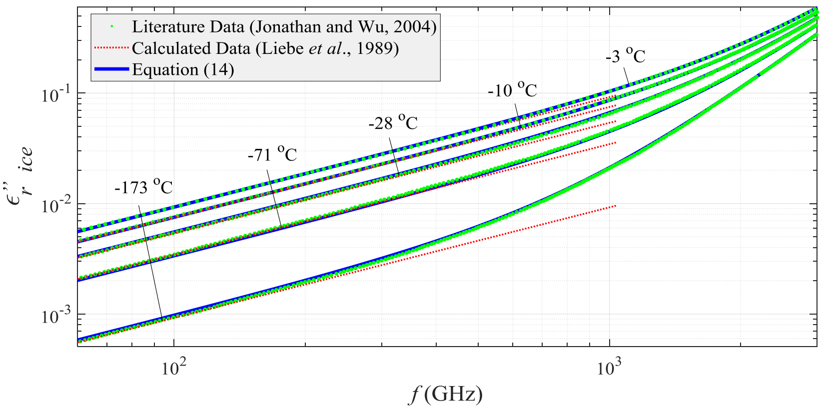

Fig. 4. Calculated ice loss factor, ε''_{r_ice} versus operating frequency, f (60 GHz to 3 THz) for temperature, T range from -3 °C to -173 °C

Below the earth's tropopause (typical h <10 km), the temperature, T changes linearly with sea level, h. The higher the h, the lower the T. Even at the same sea level, different regions of the earth have different temperatures as shown in Fig. 6 [28]. By fitting with the data in the Fig. 6, the T (in unit °C) as a functions of h (in unit meters) in the three regions are obtained.

$$T=\begin{cases} -0.006085343280028347\times h & , \quad \text{Polar} \\ -0.006279820828711083\times h+15 & , \quad \text{Middle latitude} \\ -0.005553726286337866\times h+20 & , \quad \text{Tropical} \end{cases} \tag{15}$$

Since the w of the cloud in Eq. (9) depends on the cloud's unevenness, type, and shape, as well as sea level, h [17], [29], it is difficult to accurately predict the w value in the cloud. In addition, the value of w varies with global regions [7]. Besides the area, altitude, and type of cloud factors, in general, the value of w decreases with the decrease in temperature, T [30]. Therefore, the modelling of w is not emphasized here. However, the average liquid water content, $\bar{w}$ in the cloud (in gcm^{-3}) as a function of temperature, T (in °Celsius) and pressure, P (in hPa) is given as [30].

$$\bar{w}=-1.076+\left(0.01171\times T\right)+\left(0.0002625\times P\right) \tag{16}$$

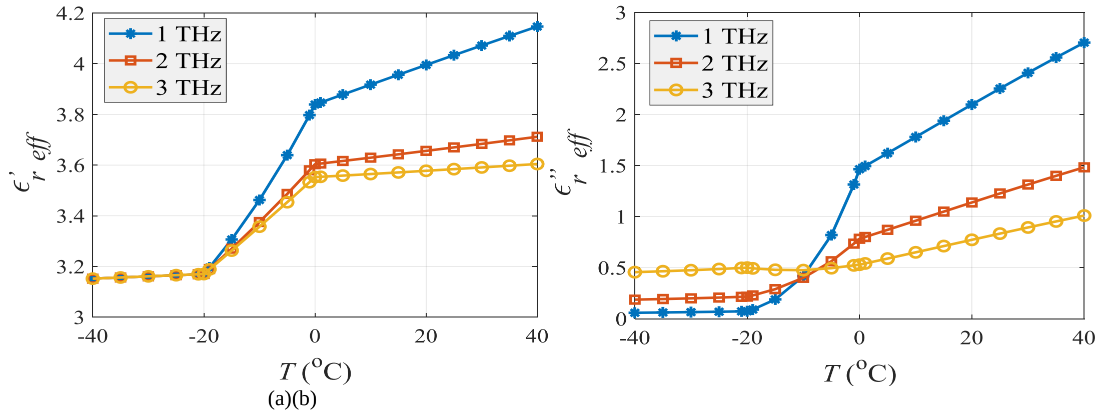

Fig. 5. Calculated (a) ε'_{r_eff} and (b) ε''_{r_eff} versus temperature, T

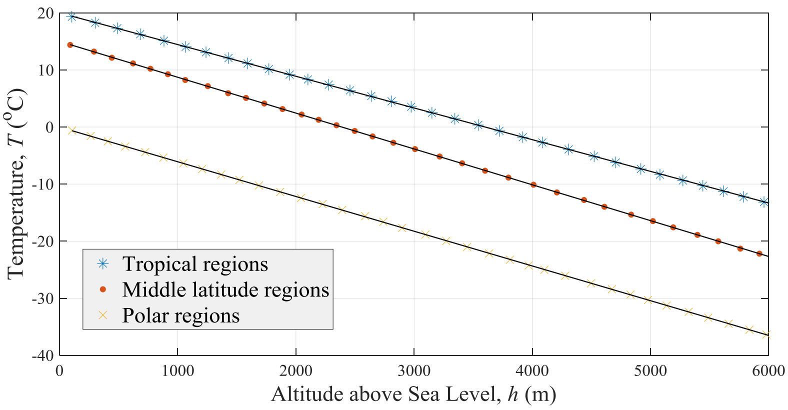

Fig. 6. Variety in above sea level, *h* with temperature, *T* in three regions of the earth

Table 3. Coefficient values of Eq. (14)

Coefficients	
ξ_1	$1.041177686355169 \times 10^{-13}$ Hz^{-1}
ξ_2	$-1.833065847883765 \times 10^{-14}$ Hz^{-1}
ξ_3	$-1.066663411303775 \times 10^{-14}$ Hz^{-1}
ξ_4	$-1.539277598578336 \times 10^{-27}$ Hz^{-2}
ξ_5	$7.644225363236554 \times 10^{-28}$ Hz^{-2}
ξ_6	$-8.865695922775403 \times 10^{-29}$ Hz^{-2}
ξ_7	$1.214522286608478 \times 10^{-38}$ Hz^{-3}
ξ_8	$-2.717923264335263 \times 10^{-40}$ Hz^{-3}
ξ_9	$4.000889228395008 \times 10^{-41}$ Hz^{-3}

The estimated absolute error of cloud attenuation, $\Delta\gamma_C$ (in dB/km) due to uncertainty values in ε'_{r_eff} and ε''_{r_eff} can be written as:

$$\Delta\gamma_C = \frac{\partial\gamma_C}{\partial\varepsilon'_{r\_eff}}\left|\Delta\varepsilon'_{r\_eff}\right| + \frac{\partial\gamma_C}{\partial\varepsilon''_{r\_eff}}\left|\Delta\varepsilon''_{r\_eff}\right| \tag{17}$$

where $|\Delta\varepsilon'_{r\_eff}|$ and $|\Delta\varepsilon''_{r\_eff}|$ are the uncertainty values in ε'_{r_eff} and ε''_{r_eff}. By solving (9) and (16), the absolute error, $\Delta\gamma_C$ can be rewritten as:

$$\Delta\gamma_C = \frac{\gamma_C}{\left[\frac{\left(\varepsilon'_{r\_eff}+2\right)^2}{\varepsilon''_{r\_eff}}+1\right]}\left\{-\left(2\varepsilon'_{r\_eff}+4\right)\left|\Delta\varepsilon'_{r\_eff}\right| + \frac{\left(\varepsilon'_{r\_eff}+2\right)^2}{\varepsilon''_{r\_eff}}\left|\Delta\varepsilon''_{r\_eff}\right|\right\} \tag{18}$$

Using Eq. (18), the change of $\Delta\gamma_C$ to the uncertainty in $|\Delta\varepsilon'_{r\_eff}|$ at 1 THz, 2 THz, and 3 THz, respectively, is calculated and plotted in Fig. 7. In this error analysis, the values of w and $|\Delta\varepsilon''_{r\_eff}|$ in (18) are fixed to be 0.3 gcm^{-3} and 0. The effect of $|\Delta\varepsilon'_{r\_eff}|$ on $\Delta\gamma_C$ is variable with operating frequency, f and temperature, T. The $\Delta\gamma_C$ will decrease when the f increases. For instance, when $|\Delta\varepsilon'_{r\_eff}| = 0.4$ exists at 0 °C, the modulus $|\Delta\gamma_C|$ will reach 1.947, 1.305, and 0.934 at 1 THz, 2 THz, and 3 THz, respectively. However, the $\Delta\gamma_C$ decreases as the temperature, T decreases. From Fig. 7, the deviation $\Delta\gamma_C$ shows a negative sign, which means that for the positive value of $|\Delta\varepsilon'_{r\_eff}|$, the predicted γ_C is less than the actual γ_C. This is because when $|\Delta\varepsilon'_{r\_eff}|$ increases with the fixed value of $|\Delta\varepsilon''_{r\_eff}|$, the atmospheric cloud will become more and more lossless (loss tangent, $\varepsilon''_{r\_eff}/\varepsilon'_{r\_eff}$ of cloud is decreases), and the attenuation of the signal propagation in the cloud will decreases. On the other hand, the deviation of $\Delta\gamma_C$ respected to the error of $|\Delta\varepsilon''_{r\_eff}|$ is plotted as shown in Fig. 8. For all frequencies, the $\Delta\gamma_C$ increases linearly with the change of $|\Delta\varepsilon''_{r\_eff}|$ for w = 0.3 gcm^{-3} and $|\Delta\varepsilon'_{r\_eff}| = 0$. When the frequency, f increases or the temperature, T decreases, the $\Delta\gamma_C$ will increase. Similarly, let $|\Delta\varepsilon''_{r\_eff}| = 0.4$ exists at 0 °C, the values of $\Delta\gamma_C$ will give 2.65, 5.96, and 9.24 at 1 THz, 2 THz, and 3 THz, respectively. Clearly, the influence of $|\Delta\varepsilon''_{r\_eff}|$ on $\Delta\gamma_C$ is greater than that of $|\Delta\varepsilon'_{r\_eff}|$, since the main natural parameter that causes microwave energy absorption and the propagation signal attenuation is the water's loss factor ε''_{r_water} in the cloud.

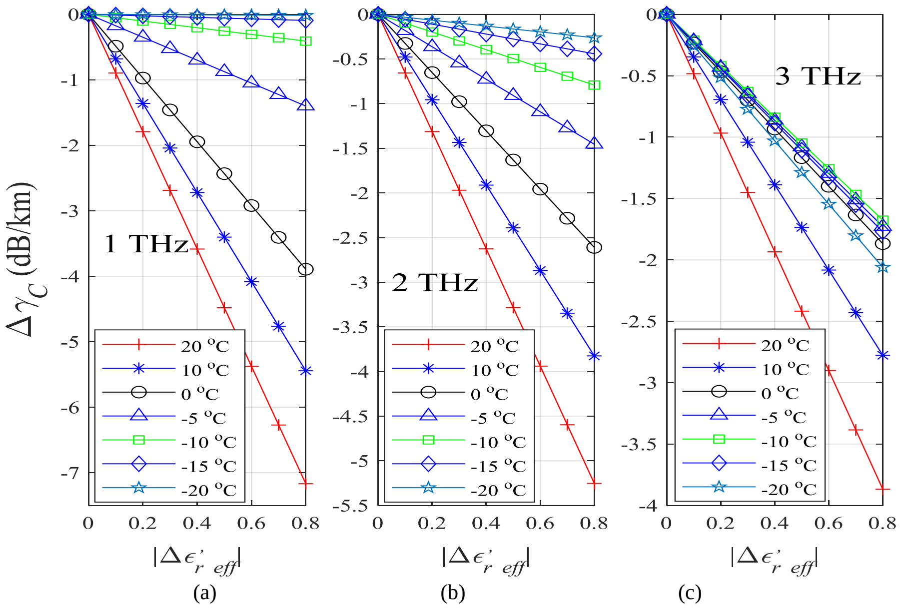

Fig. 7. Deviation of $\Delta\gamma_c$ due to the uncertainty of $|\Delta\varepsilon'_{r\_eff}|$ at (a) 1 THz, (b) 2 THz, and 3 THz, respectively (with $|\Delta\varepsilon''_{r\_eff}| = 0$ and w = 0.3 gcm^{-3})

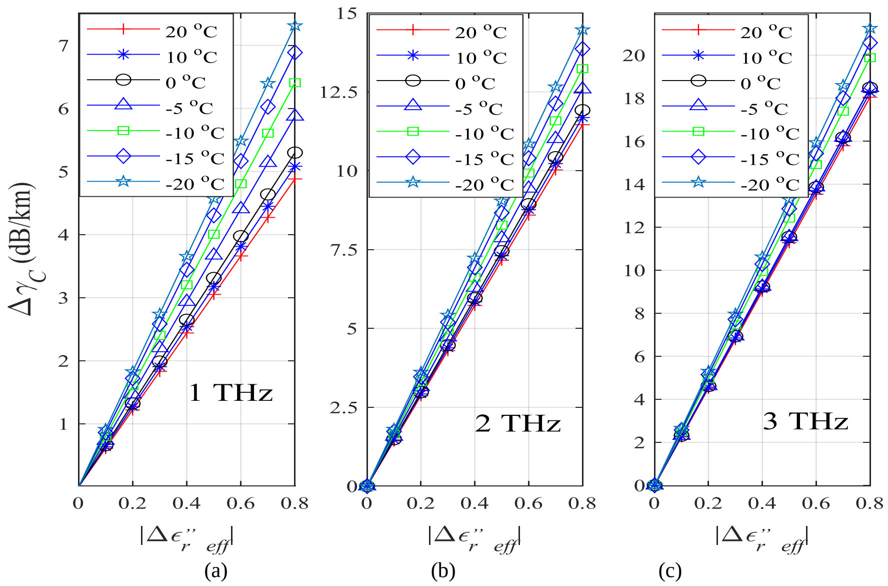

Fig. 8. Deviation of $\Delta\gamma_c$ due to the uncertainty of $|\Delta\varepsilon''_{r\_eff}|$ at (a) 1 THz, (b) 2 THz, and 3 THz, respectively (with $|\Delta\varepsilon'_{r\_eff}| = 0$ and w = 0.3 gcm^{-3})

3. Received Signal Quality

3.1 Signal-to-noise ratio (SNR)

The farther the received signal, P_r is from the noise level, P_n, the better the received signal quality. The P_r is predicted using Eq. (2). The gap level between P_r from the P_n can be evaluated using signal-to-noise ratio (SNR) as (in unit dBm):

$$\mathrm{SNR}_{(\mathrm{dBm})} = P_r - P_n = P_r - \left\{10\log_{10}\left(kT_o\right) + 30 + 10\log_{10}\left(NF\right) + 10\log_{10}\left(B\right)\right\} \tag{19}$$

where P_n (in dBm) is the noise power at the receive antenna. Symbol B (in Hertz) is the bandwidth. On the other hand, k (=1.380649×10^{-23} J/K) is the Boltzmann's constant. The NF is the noise figure value (unitless) of the receiver, which can be expressed in term of noise temperature, T_n as:

$$NF = 1 + \frac{\left(273.15 + T\right)\left(1 - 10^{-\frac{\left(A_A + A_R + A_C\right)}{10}}\right)}{T_o} \tag{20}$$

where T_o is the ambient reference temperature of 290 K. The T is the mean path physical temperature in degree Celsius (only middle latitude) at certain level of h which can be obtained from Eq. (15) [31]. On the other hand, A_A, A_R, and A_C are the atmospheric, rain, and cloud attenuations (all in unit dB), respectively, as:

$$A_A = \gamma_A \frac{d}{1000} \quad , \quad A_R = \gamma_R \frac{r \times d}{1000} \quad , \quad \text{and} \quad A_C = \gamma_C \frac{d}{1000} \tag{21}$$

3.2 Bit error rate (BER)

Apart from Eq. (19), the $\mathrm{SNR}_{(\mathrm{dBm})}$ can also be expressed in the form as:

$$\mathrm{SNR}_{(\mathrm{dBm})} = 10\log_{10}\left(\frac{E_b}{N_o}\frac{C}{B}\right) + 30 \tag{22}$$

Based on Shannon capacity theorem, the maximum rate of data, C (in unit bits per second) can be written as:

$$C = B\log_2\left(1 + 10^{\frac{\mathrm{SNR}_{(\mathrm{dBm})} - 30}{10}}\right) \tag{23}$$

From (22) and (23), the normalized signal-to-noise ratio, E_b/N_o can be calculated as:

$$\frac{E_b}{N_o} = \frac{10^{\frac{\mathrm{SNR}_{(\mathrm{dBm})} - 30}{10}}}{\log_2\left(1 + 10^{\frac{\mathrm{SNR}_{(\mathrm{dBm})} - 30}{10}}\right)} \tag{24}$$

where E_b is the energy per bit and N_o is also represented the noise power density, but in unit Watts/Hz. From Eq. (24), the bit-error rate (BER) under additive white Gaussian noise (AWGN) for various kinds of digital modulation techniques can be determined, such as amplitude shift keying (ASK), frequency shift keying (FSK), binary phase shift keying (BPSK), quadrature phase shift keying (QPSK or 4-PSK), M-array PSK, and M-array quadrature amplitude modulation (M-QAM) as listed in Table B (in Appendix B) [32].

The quantitative analysis of the relationship between logarithm value of E_b/N_o and SNR (in unit dBm) using Eq. (24) is shown in Fig. 9 (a). The E_b/N_o is almost constant and insensitive to SNR changes of less than 30 dBm. For SNR > 40 dBm, the logarithm value of E_b/N_o begins to increase linearly against SNR. On the other hand, the predicted BER based on the logarithm value of E_b/N_o for various digital modulation cases (refer to Appendix B, Table B) is illustrated in Fig. 10. For a satisfactory communication performance, the BER has to be less than 10^{-9}. However, for BER to reach the minimum acceptable level, the E_b/N_o value needs to exceed 13 dB for BPSK, QPSK, and 4-QAM, as well as exceed 16 dB for FSK, 8-PSK, and 16-QAM, respectively. For ASK, 16-PSK, and 64-QAM, the E_b/N_o value requires to reach a minimum of 21 dB. This means that SNR must exceed 50 dBm at least, since SNR = 50 dBm corresponds to $E_b/N_o \approx 13$ dB. The calculated bandwidth, B required to achieve a specific maximum data transfer rate, C with the received signal quality of SNR = 50 dBm and 60 dBm using Eq. (23), is shown in Fig. 9 (b). The future 6G communication system aims that the channel data transfer rate to reach 0.1 - 1 Tbps. If the system requires the data rate, C of 0.1 Tbsp, the bandwidth, B above 10 GHz should be used. Overall, the B required to achieve the same data transfer rate is less for the received signal with SNR = 60 dBm compared to the level of SNR = 50 dBm.

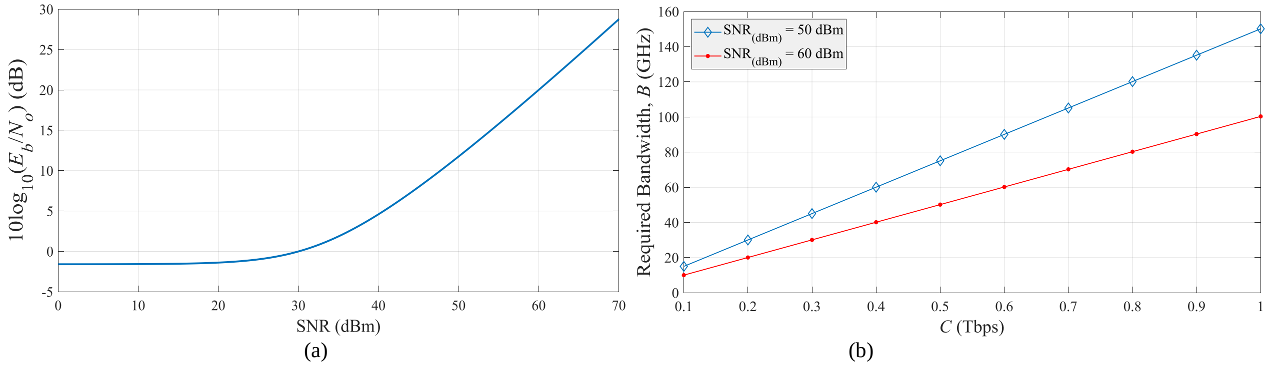

Fig. 9. (a) Relationship between E_b/N_o (in unit dB) and SNR (in unit dBm). (b) Maximum data transfer rate, C and its corresponding required bandwidth, B

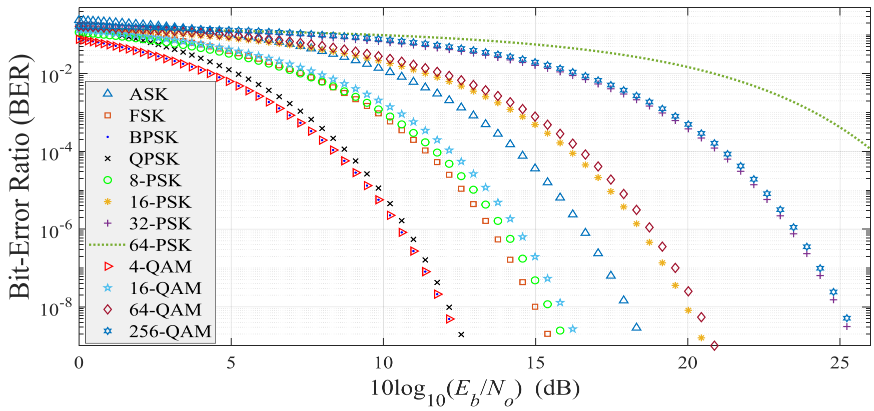

Fig. 10. Bit-error rate (BER) versus E_b/N_o (in unit dB) for different digital modulation

4. Propagation Channel App

In this study, the MATLAB-based propagation channel app is developed using '`appdesigner`' environment [33]. The app's graphical user interface (GUI) is separated to three tabs, namely 'Description Page' (Tab 1), 'Propagation Channel Simulation' (Tab 2), and 'Received Signal Quality Assessment' (Tab 3), respectively as shown in Fig. 11. The Tab 1 defines and describes the calculation configuration, symbols, parameters, and their SI units as shown in Fig. 11 (a). The Tab 2 is the main GUI page in propagation channel calculation, in which Eqs. (2)–(15) are used for the simulation as shown in Fig. 11 (b). The simulated propagation channel environment is considered to be a homogeneous atmosphere at a certain sea level, h, with uniform cloud distribution and uniform rainfall. In addition, the distance, d between the transmitter and receiver (line of sight) is considered to be always horizontal without any elevation angle. Adjustable 'knob' and 'slider' function components have been widely used in this developed app's GUI, making it easier for users to enter parameter values, especially for tablet or smartphone users with tough screen features (without physical keyboard). Besides, the 'Drop Down' component allows the user to select the operating frequency range to be simulated and the output parameters to be plotted. The display drop-down lists are shown in Fig. 11 (d). In Tab 3 [see Fig. 11 (c)], the output results are calculated using Eqs. (19)–(24) assisted with the simulated values from Tab 2. The purpose of this tab is to predict the inherent quality and maximum uncertainty in the received signal for different digital modulation methods.

Furthermore, some atmospheric parameters are also approximately predicted for reference, such as temperature, T, pressure, P, water vapour density, ρ, and relative humidity, RH, respectively [34]-[35]. It should be noted that the predicted parameters are based on the weather condition in the middle latitude regions ($22^o \le {}^o\mathrm{N} \le 45^o$). Similarly, two "drop-down" components are used for the users to select the modulation type used in the access network system and the quality evaluation parameters (SNR, BER, T_n, NF, and P_n) to be analyzed. According to the SNR or BER prediction and the specifications to be achieved, the transmit power, P_t consumption, the distance, d between the transmitter and the receiver, the altitude, h or the type of antenna used in the access network system can be re-adjusted.

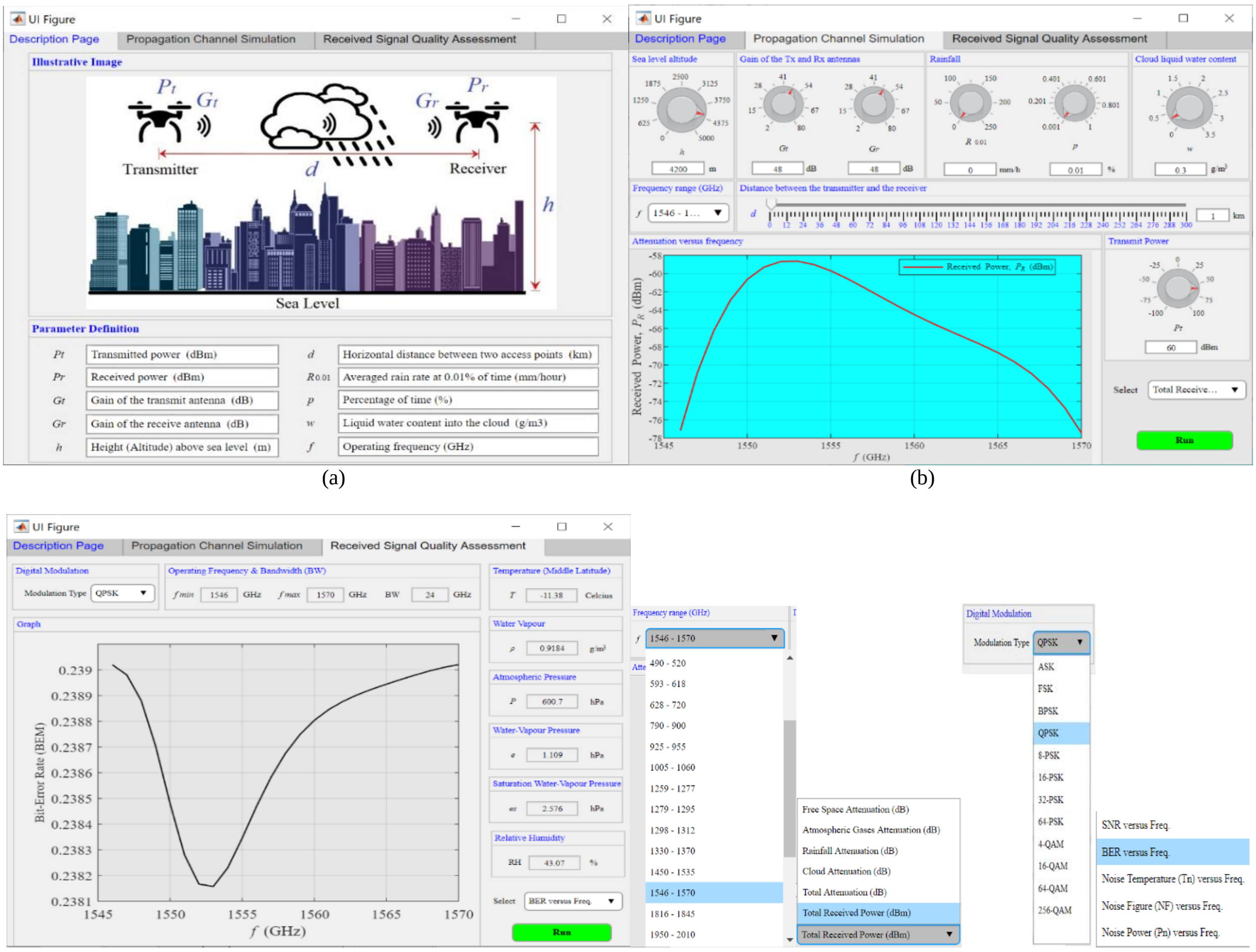

(a) (b)

(c) (d) (i) (ii) (iii) (iv)

Fig. 11. (a) Three GUI's tabs: (a) 'Description Page', (b) 'Propagation Channel Simulation', and (c) 'Received Signal Quality Assessment'. (d) Drop-down selection lists of (i) operating frequency range, (ii) plotted parameters versus frequency in 'Propagation Channel Simulation' tab, (iii) digital modulation type, and (iv) plotted parameters versus frequency in 'Received Signal Quality Assessment' tab

5. Conclusion

This paper attempts to create a simple propagation channel App based on the MATLAB GUI environment. Many of the models and data used in the App are from the recommendations of the ITU-R [2], [7], [8], [12], [15], [34], [35]. However, the origin of the ITU-R models and data are only limited up to 1 THz. In this study, the available models and data are extrapolated to 3 THz for the needs of 6G low-altitude platform non-terrestrial access networks in the future. In addition, several issues and uncertainties in the study models of attenuation due to atmospheric gases, clouds, and rain have been discussed separately. Besides, the received signal quality assessment calculations for various digital modulation systems are also included in the App. In the future, this study will be expanded to cases of non-line of sight (NLOS) propagation [36].

References

[1] Akyildiz, I. F., Kak, A., & Nie, S. (2020). 6G and beyond: The future of wireless communications systems. IEEE Access, 8, 133995–134030.
[2] ITU. (2018). Sharing between the Radio Astronomy Service and Active Services in the Frequency Range 275-3000 GHz. International Telecommunication Union Radiocommunications Sector, ITU-R Report RA.2189-1.
[3] Giordani, M., & Zorzi, M. (2021). Non-terrestrial networks in the 6G era: challenges and opportunities. IEEE Network, 35(2), 244–251.
[4] Dao, N. N., Pham, Q. V., Tu, N. H., Thanh, T. T., Bao, V. N. Q., Lakew, D. S., & Cho, S. (2021). Survey on aerial radio access networks: Toward a comprehensive 6G access infrastructure. IEEE Communications Surveys & Tutorials, 23(2), 1193–1225.
[5] Wang, A. H., Wang, P. S., Miao, X. Q., Li, X. M., Ye, N., & Liu, Y. (2020). A review on non-terrestrial wireless technologies for smart city internet of things. International Journal of Distributed Sensor Networks, 16(6), 1–17.
[6] Friis, H. T. (1946). A note on a simple transmission formula. Proceedings of the IRE, 34(5), 254–256.

[7] Attenuation Due to Clouds and Fog, International Telecommunication Union Radiocommunications Sector, Recommendation ITU-R P. 840-8, 2019.
[8] ITU. (2005). Specific Attenuation Model for Rain for Use in Prediction Methods. International Telecommunication Union Radiocommunications Sector, Recommendation ITU-R P. 838-3.
[9] Kim, I. I., Xu, S. H., & Samii, Y. R. (2013). Generalised correction to the Friis formula: quick determination of the coupling in the Fresnel region. IET Microwaves, Antennas & Propagation, 7(13), 1092–1101.
[10] Liebe, H., Hufford, G., & Cotton, M. (1993, November). Propagation modeling of moist air and suspended water/ice particles at frequencies below 1000 GHz. In Proceedings of AGARD (pp. 3-1–3-11). NASA.
[11] ITU. (2019). Attenuation by atmospheric gases and related effects, International Telecommunication Union Radiocommunications Sector, Recommendation ITU-R P. 676-12.
[12] ITU. (2008). Handbook: Radiowave Propagation Information for Designing Terrestrial Point-To-Points Links. Switzerland: International Telecommunication Union.
[13] Zufferey, C. H. (1972). A study of rain effects on electromagnetic waves in the 1-600 GHz ranges. M.S. thesis, University Colorado, Boulder, U.S., 1972.
[14] Fiorino, S., Bartell, R., Krizo, M. J., Caylor, G. L., Moore, K. P., Harris, T. R., & Cusumano, S. J. (2008, February). A first principles atmospheric propagation & characterization tool - The laser environmental effects definition and reference. In Proc. of SPIE Lasers and Applications in Science and Engineering (LASE) (pp. 1–12). SPIE.
[15] ITU. (2017). Characteristics of precipitation for propagation modelling. International Telecommunication Union Radiocommunications Sector, Recommendation ITU-R P. 837-7.
[16] Shayea, I., Rahman, T. A., Azmi, M. H., & Islam, MD. R. (2018). Real measurement study for rain attenuation conducted over 26 GHz microwave 5G link system in Malaysia. IEEE Access, 6, 19044–19064.
[17] Siles, G. A., Riera, J. M., & García-del-Pino, P. (2015). Atmospheric attenuation in wireless communication systems at millimeter and THz frequencies. IEEE Antennas and Propagation Magazine, 57(1), 48–61.
[18] Li, Q., Zhu, Q., Zheng, J. S., Liao, K. H., & Yang, G. S. (2014). Soil moisture response to rainfall in forestland and vegetable plot in Taihu Lake Basin, China. Chinese Geographical Science, 25(4), 1–12.
[19] Liebe, H. J., Manabe, T., & Hufford, G. A. (1989). Millimeter-wave attenuation and delay rates due to fog/cloud conditions. IEEE Transactions on Antennas and Propagation, 37(12), 1617–1623.
[20] Scheller, M., Jansen, C., & Koch, M. (2010). Application of effective medium theories in the Terahertz regime. In Recent Optical and Photonic Technologies (pp. 231–250). London: InTech.
[21] Salonen, E., & Uppala, S. (1991). New prediction method of cloud attenuation. Electronics Letters, 27(12), 1106–1108.
[22] Omotosho, T. V., Mandeep, J. S., & Abdullah, M. (2014). Cloud cover, cloud liquid water and cloud attenuation at Ka and V bands over equatorial climate. Meteorological Applications, 21, 777–785.
[23] Zelsmann, H. R. (1995). Temperature dependence of the optical constants for liquid H_2O and D_2O in the far IR region. Journal of Molecular Structure, 350, 95-114.
[24] Rϕnne, C., Thrane, L., Åstrand, P., Wallqvist, A., Mikkelsen, K. V., & Keiding, S. R. (1997). Investigation of the temperature dependence of dielectric relaxation in liquid water by THz reflection spectroscopy and molecular dynamics simulation. Journal of Chemical Physics, 107(14), 5319–5331.
[25] Ellison, W. J. (2007). Permittivity of pure water, at standard atmospheric pressure, over the frequency range 0 - 25 THz and the temperature range 0 - 100 ^{o}C. Journal Phys. Chem. Ref. Data, 36(1), 1–18.
[26] Jonathan, J. H., & Wu, D. L. (2004). Ice and water permittivities for millimetre and sub-millimeter remote sensing applications. Atmospheric Science Letters, 5, 146–151.
[27] Mätzler, C. (2006). Microwave dielectric properties of ice. In Thermal Microwave Radiation: Applications for Remote Sensing, Electromagn. Waves Ser., vol. 52 (pp. 455–462) U.K.: Inst. Eng. Technol.
[28] Lutgens, F. K., Tarbuck, E. J., & Tasa, D. G. (2016). The Atmosphere: An Introduction to Meteorology 13th Ed. (pp. 21). London: Pearson.
[29] Carey, L. D., Niu, J. G., Yang, P., Kankiewicz, J. A., Larson, V. E., & Haar, T. H. V. (2008). The vertical profile of liquid and ice water content in midlatitude mixed-phase altocumulus clouds. Journal of Applied Meteorology and Climatology, 47, 2487–2495.
[30] Gultepe, I., & Isaac, G. A. (1997). Liquid water content and temperature relationship from aircraft observations and its applicability to GCMs. Journal of Climate, 10, 446–452.
[31] Ho, C., Slobin, S., & Gritton, K. (2005). Atmospheric noise temperature induced by clouds and other weather phenomena at SHF band (1-45 GHz). Jet Propulsion Laboratory (JPL), California Institute of Technology, Pasadena, California, JPL D-32584.
[32] Zhang, S., Kam, P. Y., Chen, J., & Yu, C. (2010). Bit-error rate performance of coherent optical M-ary PSK/QAM using decision-aided maximum likelihood phase estimation. Optics Express, 18(12), 12088–12103.
[33] MATLAB R2020a. (2020). MATLAB App Building. U.S: MathWorks.
[34] ITU. (2017). Reference standard atmospheres, International Telecommunication Union Radiocommunications Sector, ITU-R Report P. 835-6.
[35] ITU. (2019). The radio refractive index: its formula and refractivity data, International Telecommunication Union Radiocommunications Sector, ITU-R Report P. 453-14.
[36] Oyeleke, O. D., Thomas, S., Idowu-Bismark, O., Nzerem, P., & Muhammad, I. (2020). Absorption, diffraction and free space path losses modeling for the terahertz band. I. J. Engineering and Manufacturing, 1, 54–65.

Appendix A

Table A1. Coefficient values of Eq. (5) from 275 GHz to 1060 GHz

f (GHz)	BW (GHz)	Coefficients of Eq. (5)		f (GHz)	BW (GHz)	Coefficients of Eq. (5)	
		a_1	$-2.759272940655744\times10^{-4}$			a_1	$-1.863389156377703\times10^{-4}$
275-310	35	a_2	-41.26283647067982	490-520	30	a_2	-39.53589785144725
		a_3	$-2.757044254389954\times10^{-4}$			a_3	$-1.860149411938515\times10^{-4}$
		a_4	-29.20172539760829			a_4	-27.23078805861486
		a_5	$-2.754619925266046\times10^{-4}$			a_5	$-1.857052741383811\times10^{-4}$
		a_6	-17.56657312586288			a_6	-15.35157456744144
		a_7	$-2.752035581799518\times10^{-4}$			a_7	$-1.854089755810748\times10^{-4}$
		a_8	-6.283650514212337			a_8	-3.824481719984318
		a_9	$-2.749301520429494\times10^{-4}$			a_9	$-1.851253224616656\times10^{-4}$
		a_{10}	+4.573268493265444			a_{10}	+7.276695980877381
		a_1	$-2.472975967275249\times10^{-4}$			a_1	$-2.427843333716573\times10^{-4}$
330-365	35	a_2	-40.12024353187326	593-618	25	a_2	-38.72009595789688
		a_3	$-2.472482567247289\times10^{-4}$			a_3	$-2.430061152327634\times10^{-4}$
		a_4	-27.97656527094322			a_4	-26.33790866954123
		a_5	$-2.472008078644585\times10^{-4}$			a_5	$-2.432306904353820\times10^{-4}$
		a_6	-16.25879034373557			a_6	-14.38167675410554
		a_7	$-2.471551324003089\times10^{-4}$			a_7	$-2.434579700706561\times10^{-4}$
		a_8	-4.893140883039687			a_8	-2.777612616375352
		a_9	$-2.471112408961723\times10^{-4}$			a_9	$-2.436878606631095\times10^{-4}$
		a_{10}	+6.046593682124573			a_{10}	+8.400499227468517
		a_1	$-2.236973817725231\times10^{-4}$			a_1	$-2.480413365510946\times10^{-4}$
395-425	30	a_2	-40.01219697316482	628-720	92	a_2	-40.84280858155185
		a_3	$-2.239662909323421\times10^{-4}$			a_3	$-2.481657642888589\times10^{-4}$
		a_4	-27.79682302180166			a_4	-28.41563989180597
		a_5	$-2.242378478749003\times10^{-4}$			a_5	$-2.482893874038508\times10^{-4}$
		a_6	-16.00734017405467			a_6	-16.41438098280505
		a_7	$-2.245120007215960\times10^{-4}$			a_7	$-2.484119513685460\times10^{-4}$
		a_8	-4.569962604355677			a_8	-4.765248154901047
		a_9	$-2.247889168535347\times10^{-4}$			a_9	$-2.485332792869953\times10^{-4}$
		a_{10}	+6.441526682563735			a_{10}	+6.457982053643782
		a_1	$-1.353072705549254\times10^{-4}$			a_1	$-2.266812432879295\times10^{-4}$
426-435	9	a_2	-38.33595461938549	790-900	110	a_2	-41.22905957890568
		a_3	$-1.347798402511330\times10^{-4}$			a_3	$-2.269730154261939\times10^{-4}$
		a_4	-26.10128150639765			a_4	-28.69779809043681
		a_5	$-1.342537727939308\times10^{-4}$			a_5	$-2.272810125387223\times10^{-4}$
		a_6	-14.29256321261195			a_6	-16.59246268034157
		a_7	$-1.337290238523870\times10^{-4}$			a_7	$-2.276043657828396\times10^{-4}$
		a_8	-2.836013919773095			a_8	-4.839264545727930
		a_9	$-1.332055614188750\times10^{-4}$			a_9	$-2.279427401237892\times10^{-4}$
		a_{10}	+8.194579847720217			a_{10}	+6.488025423439563
		a_1	$-1.762500792742254\times10^{-4}$			a_1	$-2.768942538415020\times10^{-4}$
456-470	14	a_2	-38.48843411969970	925-955	30	a_2	-39.28662794745976
		a_3	$-1.763295558009692\times10^{-4}$			a_3	$-2.767260479360918\times10^{-4}$
		a_4	-26.22097537305231			a_4	-26.71122767738178
		a_5	$-1.764142184128250\times10^{-4}$			a_5	$-2.765561938416166\times10^{-4}$
		a_6	-14.37945337382963			a_6	-14.56177783639927
		a_7	$-1.765040858985964\times10^{-4}$			a_7	$-2.763847970037626\times10^{-4}$
		a_8	-2.890081643340550			a_8	-2.764492889248672
		a_9	$-1.765991936491795\times10^{-4}$			a_9	$-2.762119503711143\times10^{-4}$
		a_{10}	+8.173354013789590			a_{10}	+8.606840453971836
		a_1	$-2.227436123804595\times10^{-4}$			a_1	$-2.490482780838601\times10^{-4}$
478-486	8	a_2	-37.93422494965073	1005-1060	55	a_2	-39.44630081476868
		a_3	$-2.228801296840495\times10^{-4}$			a_3	$-2.489756906812495\times10^{-4}$
		a_4	-25.64813041781908			a_4	-26.82929215155731
		a_5	$-2.230154680931005\times10^{-4}$			a_5	$-2.489035938704667\times10^{-4}$
		a_6	-13.78799596603906			a_6	-14.63822496986585
		a_7	$-2.231496252758405\times10^{-4}$			a_7	$-2.488320065513814\times10^{-4}$
		a_8	-2.280035436103469			a_8	-2.799314508656499
		a_9	$-2.232826011593203\times10^{-4}$			a_9	$-2.487609496368726\times10^{-4}$
		a_{10}	+8.801964943861556			a_{10}	+8.613651983019407

Table A2. Coefficient values of Eq. (5) from 1259 GHz to 2560 GHz

f (GHz)	BW (GHz)	Coefficients of Eq. (5)		*f* (GHz)	BW (GHz)	Coefficients of Eq. (5)	
1259-1277	18	a_1	$-1.888788917321333\times10^{-4}$	1816-1845	29	a_1	$-2.331249146370586\times10^{-4}$
		a_2	-37.97739673383337			a_2	-38.43289902291029
		a_3	$-1.888119962065421\times10^{-4}$			a_3	$-2.330055538508842\times10^{-4}$
		a_4	-25.27332996377888			a_4	-25.56825504002191
		a_5	$-1.887454974217833\times10^{-4}$			a_5	$-2.328865723560365\times10^{-4}$
		a_6	-12.99523089552555			a_6	-13.12957117768993
		a_7	$-1.886794029369518\times10^{-4}$			a_7	$-2.327679807574290\times10^{-4}$
		a_8	-1.069313257006234			a_8	-1.043061210992385
		a_9	$-1.886137214466974\times10^{-4}$			a_9	$-2.326497905403927\times10^{-4}$
		a_{10}	+10.43063680518429			a_{10}	+10.61748867097025
1279-1295	16	a_1	$-1.314037036372603\times10^{-4}$	1950-2010	60	a_1	$-2.417174155396897\times10^{-4}$
		a_2	-37.64256021294635			a_2	-39.25786867138858
		a_3	$-1.314392002817505\times10^{-4}$			a_3	$-2.416873862597603\times10^{-4}$
		a_4	-24.93069793415945			a_4	-26.35959301887215
		a_5	$-1.314749366842438\times10^{-4}$			a_5	$-2.416581977524101\times10^{-4}$
		a_6	-12.64480176481385			a_6	-13.88728702614462
		a_7	$-1.315109136450405\times10^{-4}$			a_7	$-2.416298472352043\times10^{-4}$
		a_8	-0.7110854858396576			a_8	-1.767164398197941
		a_9	$-1.315471324796352\times10^{-4}$			a_9	$-2.416023330467460\times10^{-4}$
		a_{10}	+10.79666469670111			a_{10}	+9.926988773934768
1298-1312	14	a_1	$-1.717894291281813\times10^{-4}$	2090-2130	40	a_1	$-2.206471911667611\times10^{-4}$
		a_2	-37.70519980237618			a_2	-38.97038937897975
		a_3	$-1.716944564228760\times10^{-4}$			a_3	$-2.206375012613825\times10^{-4}$
		a_4	-24.98705404081146			a_4	-26.04370233188422
		a_5	$-1.716000319610287\times10^{-4}$			a_5	$-2.206290454281548\times10^{-4}$
		a_6	-12.69487466714233			a_6	-13.54297158078130
		a_7	$-1.715061567654041\times10^{-4}$			a_7	$-2.206218193190116\times10^{-4}$
		a_8	-0.7548754748263384			a_8	-1.394411011895746
		a_9	$-1.714128322859846\times10^{-4}$			a_9	$-2.206158200955188\times10^{-4}$
		a_{10}	+10.75915731777107			a_{10}	+10.32819308603489
1330-1370	40	a_1	$-1.689117268841746\times10^{-4}$	2285-2316	31	a_1	$-2.316119857348792\times10^{-4}$
		a_2	-39.50232494244032			a_2	-37.77805245516939
		a_3	$-1.689384504456426\times10^{-4}$			a_3	$-2.315704659806097\times10^{-4}$
		a_4	-26.76912452081995			a_4	-24.81459946582781
		a_5	$-1.689706689457493\times10^{-4}$			a_5	$-2.315291195388288\times10^{-4}$
		a_6	-14.46186360532601			a_6	-12.27711395818090
		a_7	$-1.690083340775304\times10^{-4}$			a_7	$-2.314879486472590\times10^{-4}$
		a_8	-2.506756341404365			a_8	-0.09180968495336432
		a_9	$-1.690514191723862\times10^{-4}$			a_9	$-2.314469556697869\times10^{-4}$
		a_{10}	+9.022410862602369			a_{10}	+11.66752717496451
1450-1535	85	a_1	$-2.818368518296465\times10^{-4}$	2322-2332	10	a_1	$-2.693317965091296\times10^{-4}$
		a_2	-40.08744852664764			a_2	-36.47119463601496
		a_3	$-2.819379739551620\times10^{-4}$			a_3	$-2.693707218248153\times10^{-4}$
		a_4	-27.31061641441497			a_4	-23.50210823063184
		a_5	$-2.820350165875636\times10^{-4}$			a_5	$-2.694096132487244\times10^{-4}$
		a_6	-14.95976587617088			a_6	-10.95899030410055
		a_7	$-2.821280057601026\times10^{-4}$			a_7	$-2.694484706570117\times10^{-4}$
		a_8	-2.961110476023925			a_8	+1.231945356579091
		a_9	$-2.822169398747085\times10^{-4}$			a_9	$-2.694872939267367\times10^{-4}$
		a_{10}	+8.611564247622313			a_{10}	+12.99691253620697
1546-1570	24	a_1	$-2.399930383738839\times10^{-4}$	2490-2560	70	a_1	$-2.584435121010365\times10^{-4}$
		a_2	-38.10404284705749			a_2	-39.40763590876102
		a_3	$-2.399837734522424\times10^{-4}$			a_3	$-2.584360754006805\times10^{-4}$
		a_4	-25.30882963322675			a_4	-26.40278082078309
		a_5	$-2.399748136072810\times10^{-4}$			a_5	$-2.584289832720625\times10^{-4}$
		a_6	-12.93958510387853			a_6	-13.82388923869504
		a_7	$-2.399661569067241\times10^{-4}$			a_7	$-2.584222338405925\times10^{-4}$
		a_8	-0.9225230858961576			a_8	-1.597174978706321
		a_9	$-2.399578015989522\times10^{-4}$			a_9	$-2.584158250183469\times10^{-4}$
		a_{10}	+10.66857017194022			a_{10}	+10.20357575261026

Table A3. Coefficient values of Eq. (5) from 2570 GHz to 2045 GHz

f (GHz)	BW (GHz)	Coefficients of Eq. (5)		f (GHz)	BW (GHz)	Coefficients of Eq. (5)	
2570-2600	30	a_1	$-2.952296078922083\times10^{-4}$	2810-2865	55	a_1	$-2.417865259144426\times10^{-4}$
		a_2	-37.82849663185917			a_2	-38.57552113063817
		a_3	$-2.952470786472076\times10^{-4}$			a_3	$-2.417566873972409\times10^{-4}$
		a_4	-24.81315100051005			a_4	-25.52074789200217
		a_5	$-2.952641572306955\times10^{-4}$			a_5	$-2.417272179758349\times10^{-4}$
		a_6	-12.22377279631590			a_6	-12.89194049288401
		a_7	$-2.952808478727771\times10^{-4}$			a_7	$-2.416981166999073\times10^{-4}$
		a_8	$+0.01342416477694755$			a_8	-0.6153126797159040
		a_9	$-2.952971546219089\times10^{-4}$			a_9	$-2.416693827774005\times10^{-4}$
		a_{10}	$+11.82465364049239$			a_{10}	$+11.23534937994082$
2700-2735	35	a_1	$-2.764835087785051\times10^{-4}$	2895-2945	50	a_1	$-2.700647194879143\times10^{-4}$
		a_2	-38.15167494972184			a_2	-38.32719500781999
		a_3	$-2.764897805318294\times10^{-4}$			a_3	$-2.701496626756446\times10^{-4}$
		a_4	-25.11519155816109			a_4	-25.25929342650967
		a_5	$-2.764957278755737\times10^{-4}$			a_5	$-2.702341362885896\times10^{-4}$
		a_6	-12.50467426525840			a_6	-12.61735562440492
		a_7	$-2.765013529074023\times10^{-4}$			a_7	$-2.703181396112760\times10^{-4}$
		a_8	-0.2463368711728663			a_8	-0.3275954356193449
		a_9	$-2.765066574665420\times10^{-4}$			a_9	$-2.704016718876303\times10^{-4}$
		a_{10}	$+11.58603439953573$			a_{10}	$+11.53620088148817$

Appendix B

It should be noted that M (= 4, 16, 32, 64, or 256) is the constellation size and 'erfc' is the complementary error function which is defined as:

$$\mathrm{erfc}(z) = \frac{2}{\sqrt{\pi}} \int_z^{\infty} e^{-t^2} \partial t$$

Table B. Bit-error rate models [35]

Type	Bit-error rate (BER)	Type	Bit-error rate (BER)
ASK	$\mathrm{BER} = \frac{1}{2}\mathrm{erfc}\left(\sqrt{\frac{E_b}{4N_o}}\right)$ (B1)	QPSK	$\mathrm{BER} = \mathrm{erfc}\left(\sqrt{\frac{E_b}{N_o}}\right)$ (B4)
FSK	$\mathrm{BER} = \frac{1}{2}\mathrm{erfc}\left(\sqrt{\frac{E_b}{2N_o}}\right)$ (B2)	M-ary PSK (M >4)	$\mathrm{BER} = \frac{1}{\log_2 M}\mathrm{erfc}\left\{\sqrt{\frac{E_b}{N_o}\log_2 M}\sin\left(\frac{\pi}{M}\right)\right\}$ (B5)
BPSK	$\mathrm{BER} = \frac{1}{2}\mathrm{erfc}\left(\sqrt{\frac{E_b}{N_o}}\right)$ (B3)	M-QAM	$\mathrm{BER} = 1 - \left\{1 - \frac{\left(1-\frac{1}{\sqrt{M}}\right)}{\log_2 M}\mathrm{erfc}\left(\sqrt{\frac{E_b}{N_o}\frac{3}{2(M-1)}\log_2 M}\right)\right\}^2$ (B6)

Authors' Profiles

Kok Yeow You was born in 1977. He obtained his B.Sc. Physics (Honours) degree in Universiti Kebangsaan Malaysia (UKM) in 2001. He pursued his M.Sc. in Microwave at the Faculty of Science in 2003 and his Ph.D. in Wave Propagation at the Institute for Mathematical Research in 2006 in Universiti Putra Malaysia (UPM), Serdang, Selangor, Malaysia. Recently, he is a senior lecturer at School of Electrical Engineering, Faculty of Engineering, Universiti Teknologi Malaysia (UTM), Skudai, Johor, Malaysia. His main personnel research interest is in the theory, simulation, and instrumentation of electromagnetic wave propagation at microwave/millimeter-wave frequencies focusing on the modeling and development of microwave passive components, wireless communication devices, and sensors for medical and agricultural applications.

How to cite this paper: Kok Yeow You, "Propagation Channel Modeling for Low-Altitude Platform Non-Terrestrial Networks from 275 GHz to 3 THz", International Journal of Wireless and Microwave Technologies(IJWMT), Vol.12, No.3, pp. 1-17, 2022.DOI: 10.5815/ijwmt.2022.03.01